ENHANCED EFFICIENCY AND FLIGHT ENVELOPE BY VARIABLE MAIN ROTOR SPEED FOR DIFFERENT HELICOPTER CONFIGURATIONS

W. Garre[1], T. Pflumm, M. Hajek,
Institute of Helicopter Technology, Technical University of Munich, D-85748 Garching, Germany

Abstract

Today, most rotorcraft are operated at constant rotor speeds. Recent studies show that a variable rotor speed increases the efficiency and extends the flight envelope of rotorcraft [1]–[3]. With a variable rotor speed, rotorcraft can be developed and optimized for a whole operational design range rather than a specific design point. Funded by the German Aviation Research Program (LuFo V-2) and the Austrian Research Program TAKE OFF, the project VARI-SPEED intends to give answers about the applicability and the determination of decision factors of such a technology. In this study the effects of a variable-speed rotor design on power savings and flight envelope are discussed for various existing helicopter configurations. Calculations were performed using NDARC (NASA Design and Analysis of Rotorcraft). The aircraft chosen for the study are the UH-60A single main-rotor and tail-rotor helicopter, the CH-47D tandem helicopter, the XH-59A coaxial lift-offset helicopter and the XV-15 tiltrotor. Areas of possible power savings, ranges of rotational speed and main-rotor torque effects are presented. The effects of additional transmission weight are also highlighted. Depending on the aircraft, significant power savings are possible at certain flight regimes.

SYMBOLS AND ABBREVIATIONS

EW	[lb]	empty weight
GW	[lb]	gross weight
MCP	[hp]	maximum continuous power
MTOW	[lb]	maximum take of weight
TW	[lb]	transmission weight
A	[ft^2]	rotor disc area
C_P	[-]	power coefficient
C_T/σ	[-]	blade loading
V_{tip}	[ft/sec]	rotor tip speed
V_f	[kts]	cruise speed
κ	[-]	inflow factor
μ	[-]	advance ratio
ρ	[kg/m^3]	density
σ	[-]	solidity
$(.)_{ref}$		reference configuration

INTRODUCTION

To meet future vertical lift requirements of high-lift and high-speed cruise with low noise and vibrations, the NASA Heavy Lift Rotorcraft Systems Investigation [4] has identified the need for advanced variable speed drive systems to better match hover and cruise flight conditions. Under ecological aspects a variable rotor speed offers the opportunity to operate the rotor at an optimal pitch to improve fuel efficiency and reduced noise radiation. An example of a helicopter incorporating the idea of a variable rotor speed is the Boeing A160T Hummingbird that uses a two-speed transmission to expand the flight envelope to higher gross weights or altitudes [5], [6]. High speed compound configurations such as the Eurocopter X^3, the ABC™ (Advancing Blade Concept) demonstrator XH-59A [7], Sikorsky X2 [8] and the lately introduced Sikorsky S-97 Raider make use of a slowed rotor to avoid compressibility effects during fast forward flights. Similar to the experimental compound configurations that change the rotor angular velocity to increase the maximum forward speed, tiltrotor concepts such as the Bell XV-15 demonstrator and the Bell Boeing V-22 Osprey vary rotor speed between helicopter and aircraft mode. Such technology requires a well-designed rotor system and preferably a gear box that supports variable speed transmission to the rotor shaft while having a constant engine shaft speed.

The project VARI-SPEED intends to give answers about the applicability and determination of decision factors of variable speed transmissions and rotor sys-

[1] w.garre@tum.de; +49 (0)89/289-16359; www.ht.mw.tum.de

tem for future vertical lift aircraft. This study targets several objectives in this context:

- study different helicopter configurations
- gain insight into the sensitivity of variable rotor speed helicopter designs and its effect to the flight envelope
- gain knowledge about possible power savings for selected flight states
- analyze necessary rotational speed bandwidths, and effects on mean main-rotor torque
- estimate the effects of additional transmission weights

Not examined in this work are effects on noise, costs, feasibility, etc..
To achieve these goals, a methodology was chosen that validates existing configurations against flight test data with a subsequent variation of rotor speed. This strategy was selected over a method that completes a sizing task comprising significant uncertainties but covering the full potential of variable rotor speed technology and allowing a comparison of different configurations.
While this may not reveal the full potential of the technology, the importance of validated performance calculations are essential for the first part of the project. Later in the project it is intended to design a rotor and transmission system for a selected configuration to investigate structural and vibrational problems encountered by a variable rotor speed. Stability and feasibility will then be studied as well as a proof of concept.

Performance calculations are performed with NDARC [9], [10]. Advantages of the software are the low demand of computational resources, short run-time, well documented examples and the possibility to easily add or remove aircraft components. The handling of required input for each helicopter is appropriate. Several rotorcraft configurations are considered within this study to cover various rotor operating conditions not occurring distinctly at common main-/ tail-rotor configurations. For instance lift offset, high advancing ratios, high discload and altering airplane propeller and helicopter mode are of special interest regarding variable rotor speed advantages. The aircraft chosen for the study are the UH-60A single main-rotor and tail-rotor helicopter, the CH-47D tandem helicopter, the XH-59A coaxial lift-offset helicopter and the XV-15 tiltrotor, shown in figure 1.

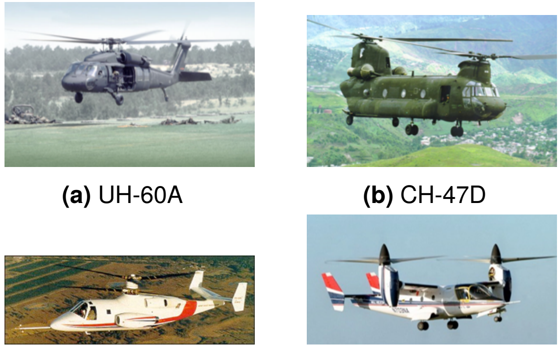

(a) UH-60A **(b)** CH-47D

(c) XH-59A **(d)** XV-15

Figure 1: considered configurations [10]

METHODOLOGY

NDARC is based on an advanced momentum theory. The required power is assumed as sum of component power P_{comp}, transmission losses P_{xmsx} and accessory losses P_{acc}, described in equation (1). The component power, equation (2), is the sum of induced, profile, interference and parasite power terms [10] in level flight. The distinct power components are enhanced by surrogate models to incorporate rotor performance characteristics beyond the classical momentum theory [9]. This adjustment uses non-dimensional rotor parameters to account for aerodynamic phenomena that are usually neglected. The induced power, equation (3), is calculated from the ideal induced velocity with the empirical factor κ to account for non-uniform inflow, non-ideal span loading, tip losses, swirl, blockage, and other phenomena [9]. The empirical factor κ is modeled as a function of advance ratio μ and blade loading C_T/σ, instead of being a constant correctional factor. Similarly, the profile power, equation (4), is calculated assuming a non-constant mean drag-coefficient $c_{d,mean}$ to account for a better power estimation with stall- and compressibility as well as Reynolds number corrections [9]. F_P takes into account the additional speed at a blade section due to edgewise and axial flight.

(1) $$P_{req} = P_{comp} + P_{xmsx} + P_{acc}$$

(2) $$P_{comp} = P_i + P_0 + P_t + P_p$$

(3) $$P_i = \kappa P_{i,ideal}$$

(4) $$P_0 = \rho A V_{tip}^3 C_{p0}$$

(5) $$\text{with: } C_{p0} = \left(\frac{\sigma}{8}\right) c_{d,mean} F_P$$

(6) $$\text{with: } c_{d,mean} = f\left(\frac{C_T}{\sigma}, \mu, \ldots\right)$$

The successful use of the underlying surrogate-model requires a careful selection of the input parameters. The calibration of parameters for existing aircraft is therefore an inevitable process. Fortunately, Johnson [10] provides an extensive calibration and validation for the aircraft of this study, which states the baseline of the aircraft description. Johnson used geometry and weight information of the aircraft with airframe wind tunnel test data, engine decks and rotor performance tests together with comprehensive analysis results from CAMRAD II (Comprehensive Analytical Model of Rotorcraft Aerodynamics and Dynamics). Nevertheless, all configurations are again validated against flight test data with the goal to determine and verify the selection of surrogate parameters for κ, $c_{d,mean}$ and parasitic drag as a function of inflow, blade loading, advance ratio, Mach number, etc.. Values were selected and fitted to better match the flight test results within boundaries defined from a physical sense to minimize a least squares error.

The UH-60A is validated against a NDARC model from Johnson [10] and flight test data from Bousman [11] and Nagata [12]. Note that the UH-60A is modeled without movable horizontal stabilizer. Even in hover, its incidence is fixed to forward flight setup. Figure 2 and 3 show the required power as well as induced and profile power plotted over three different blade loadings. The figures show that the power breakdown of the UH-60A corresponds well to the reference data.

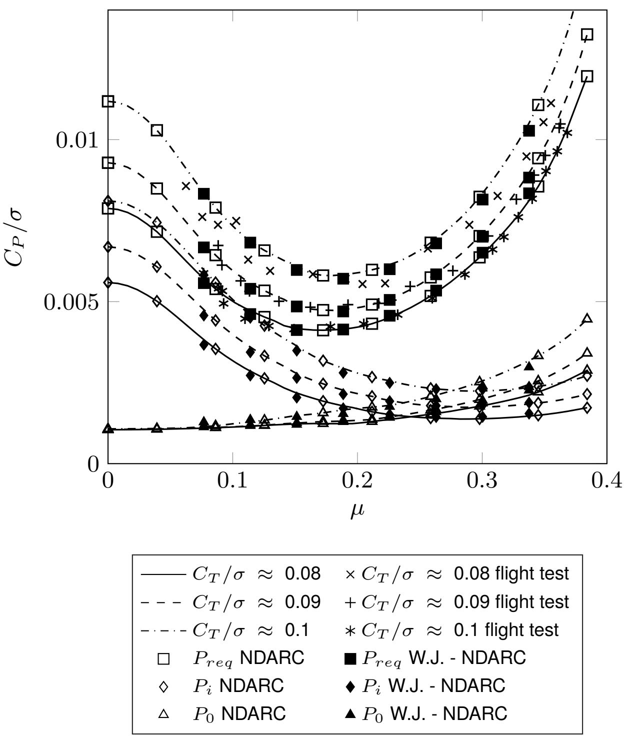

Figure 2: NDARC UH-60A cruise flight performance validation in comparison to Johnson [10] and flight test data [11]

In consequence of the comprehensive fight test data of the CH-47D tandem configuration from Bender[13],

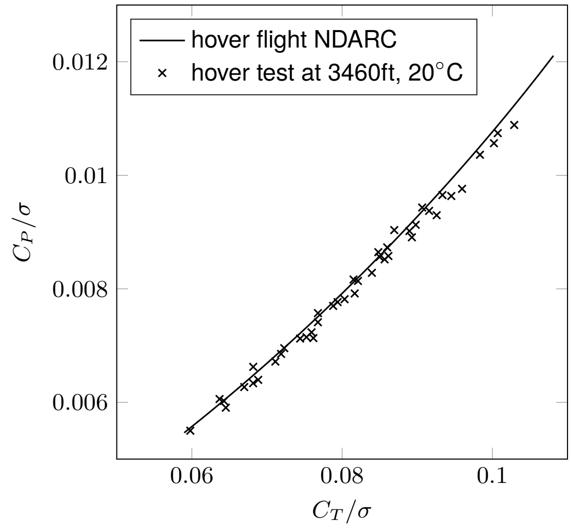

Figure 3: NDARC UH-60A hover performance validation in comparison to Johnson [10] and flight test data [12]

at different gross weights, altitudes and even rotational speeds, the NDARC model was verified with great confidence. Simplifications were made for the trim law, which neglect the longitudinal cyclic pitch.

The coaxial lift-offset helicopter XH-59A is considered as both coaxial helicopter and compound configuration with two jet engines as auxiliary propulsion within this study. The goal of the XH-59A experimental program was solely to demonstrate the feasibility of the Advancing Blade Concept (ABC^{TM}) rotor technology and use as a research tool for investigation of rotor characteristics with and without auxiliary propulsion because the rotor design has unique impacts on controllability, noise, loads and dynamics [7]. Especially in terms of shaft angle and blade twist, the rotor was therefore a design compromise to realize both configurations [7]. Analog to the previous helicopters, the goal was to determine a set of surrogate parameters that are valid for both the coaxial and the compound configuration with additional auxiliary pushers. The XH-59A is validated against NDARC calculations from Johnson [10] and flight test data from Arents [14], Ruddell [15], [16] and Pleasants [17]. The auxiliary jets are considered as simple force generators. Again, surrogate parameters are selected and fitted to better match the flight test results within defined physical boundaries.

The main-rotor power of the compound configuration is reduced with increasing advance ratio, because the power of the auxiliary pusher increase significantly with advance ratio [18]. Consequently, every modern high speed ABC compound configuration would therefore use one propulsion system for the main rotor and the pusher [7]. Hence, the jet engines of the

XH-59A where replaced for the VARI-SPEED study with a 6 bladed pusher tail-rotor that corresponds to the dimensions of Sikorsky S-97 Raider with a diameter of 7 feet and a solidity of $\sigma = 0.16$. It is centrally mounted at the rear of the tail-boom.

The XV-15 is an experimental tiltrotor aircraft with vertical take off and landing capabilities. The aircraft is validated against NDARC and CAMRAD II calculations from Johnson [10] and published flight test data from Acree [19], [20] and Maisel [21]. Readapting the NDARC surrogate parameters to match CAMRAD II calculation from Johnson [10] with a subsequent verification of the required power and trim state of the aircraft showed good agreement with flight test data in both helicopter and aircraft mode.

Flight speed, altitude, gross weight and rotor speed are spanning a 4-dimensional field of trimmed flight state solutions bounded by the convergence limit of NDARC. The limit depends on the configuration and makes a coordinated, looped calculation of all flight states difficult. A recursive approach is chosen instead, as the convergence of a single flight state depends strongly on the starting condition. After a flight state is calculated, the trim variables (control inputs & attitude) are given to the subsequent calculation as start condition. Trim algorithms are utilized in NDARC to solve rotor flapping dynamics and flight attitude. In the 4-dimensional space each calculation has 8 direct neighbors. A resolution of 30 discrete points in each dimension was selected, while the rotor speed was discretized at 50 points in an interval of $\pm$50% of the reference speed which results in more than 10^6 flight states for each aircraft. Hover and level flight at ISA (International Standard Atmosphere) conditions are considered exclusively within the study.

The discrete calculations over a wide range of rotor speed eases the optimization problem of finding the related optimal rotor speed. It is determined by selecting the flight state with the minimum required power at each point in the flight envelope. This approach also allows an investigations on the variation of rotor speed in the neighborhood of the optimum value, which gives valuable insight and possible performance indicators. From linear interpolation the point performances can be derived at any arbitrary point.

Rotor specific states are commonly used to illustrate power and flight envelope improvements for helicopters, due to the fact that the main-rotor is the most influential part. Because blade loading and advance ratio are well-established rotor parameters and a function of blade tip-speed, a normalization is applied to ensure comparability with the reference tip-speed, given by:

$$\left(\frac{C_T}{\sigma}\right)_{ref} := \left(\frac{C_T}{\sigma}\right) \cdot \left(\frac{V_{tip}}{V_{tip,ref}}\right)^2 \tag{7}$$

$$\mu_{ref} := \mu \cdot \left(\frac{V_{tip}}{V_{tip,ref}}\right) \tag{8}$$

Power savings, ranges of rotational speed and main rotor torque effects are hereinafter used in the following definition:

$$\Delta P = \frac{P_{req,ref} - P_{req}}{P_{req,ref}} \cdot 100 \tag{9}$$

$$\Delta V_{tip} = \frac{V_{tip} - V_{tip,ref}}{V_{tip,ref}} \cdot 100 \tag{10}$$

$$\Delta Q = \frac{Q - Q_{ref}}{Q_{ref}} \cdot 100 \tag{11}$$

A change of main-rotor torque will lead to a change of drive train weight. As a major objective of the associated project VARI-SPEED is to determine the most promising configuration and related flight states for variable rotor speed, provided by a variable transmission, another key feature for drive train weight increase is resulting from enabling variable rotor speed by an additional transmission stage. Therefore, a transmission weight increase and its trade-off against power savings is considered. The required reduction of payload to keep the power demand at a constant level is not the focus of interest, but the increased power demand keeping payload constant is. Nevertheless, the MTOW is still limiting the payload capacity. Impacts on structural weight increase are neglected. Figure 4 illustrates how additional transmission weight ΔTW is taken into account for a cruise speed range. For each state the power demand at reference rotor speed is compared to the power demand with additional weight at optimal rotor speed. The empty weigt of the optimal rotor speed configuration increases by ΔTW. Related impacts are studied for a transmission weight increase of both 10% and 30%.

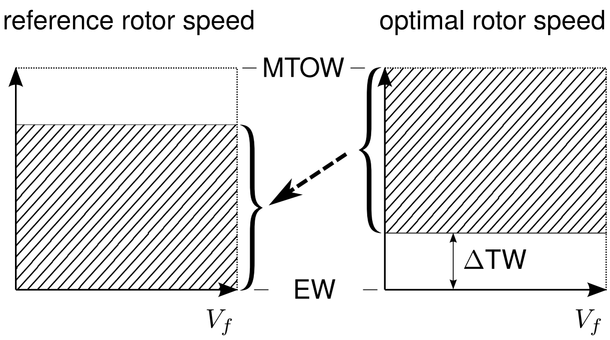

Figure 4: Illustration of how additional TW is trade off against optimal rotor speed.

RESULTS

First of all, the potential of a variable main-rotor speed is outlined in hover flight. This eases the evaluation of the multiple dimensions covered by the calculation. The UH-60A is used to outline characteristics of variable rotor speed. The other helicopters, considered in this study, are compared against the UH-60A and differences are highlighted. At first the investigation focuses on effects caused by altering blade loading. Altering advance ratios are investigated later on.

The Figure of Merit (FM) turned out to be no suitable indicator for hover performance in association with variable main-rotor speed. As the required power rather than the FM was optimized to achieve the optimal rotor speed in hover flight, the FM does not represent the total power optimum at variational rotor speed. The power coefficient is neither suitable for variable rotor speed investigations, because it would lead to misinterpretations as a varying rotor speed influences the power coefficient. The blade loading is influenced in the same manner. As a result the thrust correlates negatively with blade loading, as the optimal rotor speed is obtained to increase with main rotor thrust. Therefore, the blade loading is neither suitable.

Adjusting the main-rotor speed entails individual effects on the power components. In hover, at reference rotor speed the induced power is dominating the total power demand by approximately 65-70% within the engine limit. The amount of profile power is 14-20%. The induced power does not significantly change with rotor speed adjustment, because both, the required thrust and the related induced velocity are not significantly affected by rotor speed variation. Instead, the profile power can be reduced by approximately -40% to -60%. Thus, power savings are significantly depending on the amount of P_0. As the ratio between profile power and required power increases with horizontal speed, it is expected to gain more power savings in forward flight.

Figure 5 illustrates the required power over the blade loading and main-rotor speed at hover flight. The rotor speed covers a range of $\pm$50% in relation to the reference tip-speed of 725ft/sec. The maximum blade loading represents a gross weight of 19000lb at 17000ft. The minimum blade loading represents the empty weight at sea level. In between both high and low blade loading the evaluation is supported at 23 points, linear distributed in both weight and altitude. The engine limit covers approximately the lower third of blade loading. The power is illustrated by iso-lines. At low blade loading these iso-lines show a flat maximum and a sharper maximum at high blade

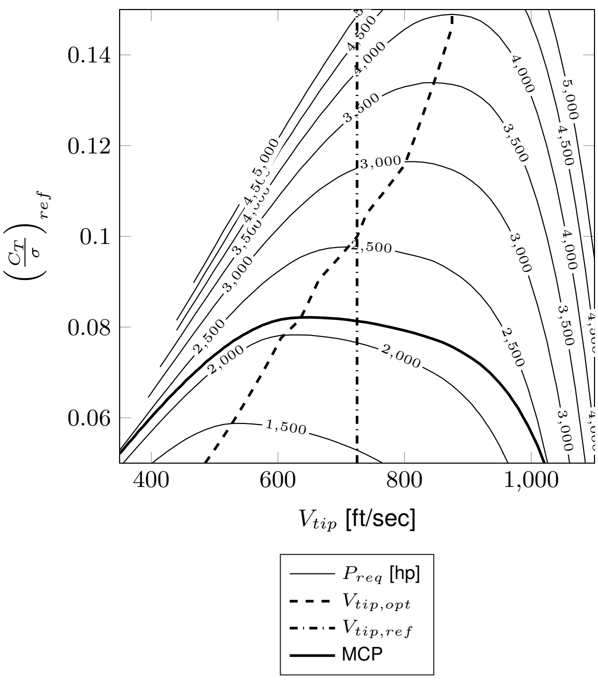

Figure 5: The required hover power over main-rotor tip-speed and normalized blade loading for the UH-60A.

loading. Because of the single optimum only, one optimal rotor speed exists, which is approximately 30% lower than the reference rotor speed at low blade loading. At high blade loading the optimal rotor speed is approximately 30% higher than the reference. It is remarkable that the blade loading level is beyond the engine limit, where the reference rotor speed is the optimal speed. Thus, within the engine limit power savings are achievable at any blade loading. The main-rotor speed is not perfectly designed to provide optimal hover performance. But as the power-gradient with respect to the rotor speed is low within the engine limit, the optimum has almost been reached at reference rotor speed. Obviously, a wide range of rotor speed is required to maintain maximum power savings especially at low blade loading within the engine limit. Regimes of a higher gradient which particularly require a rotor speed adjustment are existing predominately at high blade loading and are exceeding the engine limit.

The shape of the power optimum is of no concern in the following investigations. Power savings and the related tip-speed are always calculated regarding the optimum. To have a better insight towards the means of power savings, these are illustrated in figure 6 over the blade loading. In both hover and cruise flight especially at low and high normalized blade loading power savings are possible. At $(C_T/\sigma)_{ref} = 0.1$, $(C_T/\sigma)_{ref} = 0.09$ resp. power savings vanish due to the optimized helicopter design in these points. In hover flight power savings up to 12% are possible

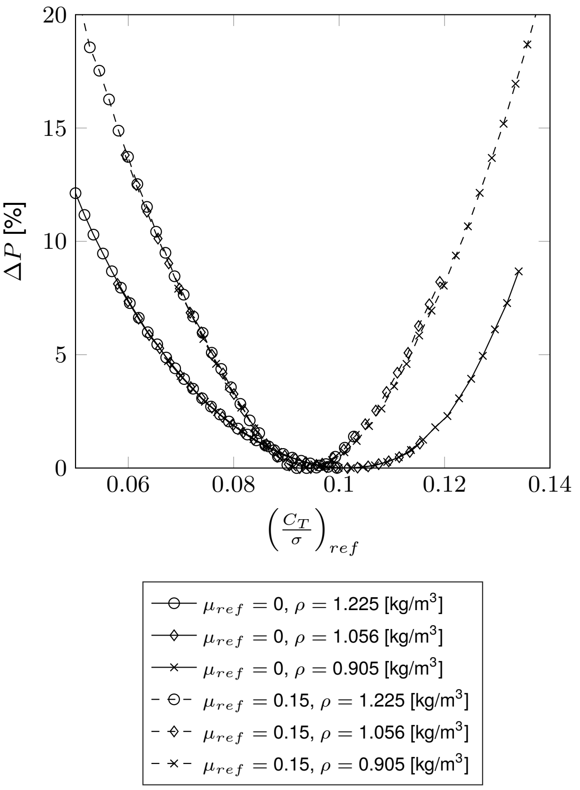

Figure 6: Power savings of the UH-60A over the normalized blade loading for both, hover and cruise flight at three different altitudes.

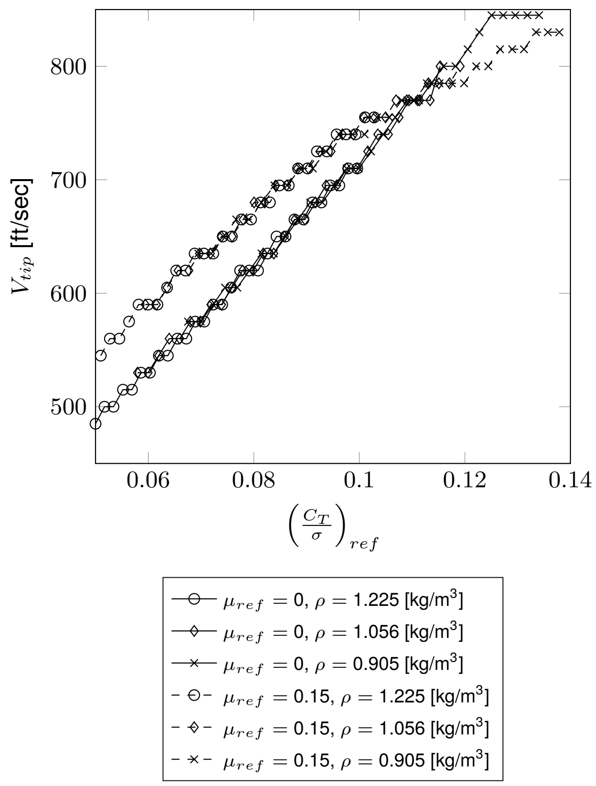

Figure 7: Optimal rotor speed of the UH-60A over the normalized blade loading for both, hover and cruise flight at three different altitudes.

within the engine limit, approximately located at $(C_T/\sigma)_{ref} = 0.08$. Beyond this limit, the power savings are less than 2% in a wide range up to a blade loading of $(C_T/\sigma)_{ref} = 0.12$. Thus, the benefit of variable rotor speed is limited in this range. At $\mu_{ref} = 0.15$ power savings up to 20% are possible within the engine limit, located at $(C_T/\sigma)_{ref} = 0.12$.

Obviously, the power savings are only depending on normalized blade loading in hover. This is a remarkable feature that means that the potential of the variable rotor speed technology is not principally associated to flight altitude and gross weight but to combinations of both. More remarkable is that the rotor speed behaves in a same manner in hover, as illustrated in figure 7. The stairs-like appearance results from the calculation of discrete rotor speeds. The optimal rotor speed equally depends only on $(C_T/\sigma)_{ref}$ but not on the altitude and the specific gross weight, for both in combination the normalized blade loading has been reached. Regarding the blade loading, a strictly monotonically increasing trend of the optimal rotor speed exists. With increasing flight speed, contrary to expectations, the optimal rotor speed increases even beyond both illustrated advancing ratios. Power savings and optimal rotor speed are thus depending significantly on rotor states rather than on overall system states. This is reasonable by considering that rotor speed adjustment has primarily an effect on the rotor itself. The reason for the density having no influence on power savings at constant normalized blade loading regarding the reference rotor speed is explained in the following. Claiming $(C_T/\sigma)_{ref} = const.$ the rotor speed is approximately constant with respect to figure 7. Both aspects together are leading to the following characteristics in hover flight.

$$P_i\left(\left(\frac{C_T}{\sigma}\right)_{ref} = const., V_{tip} = const.\right) \propto \rho \tag{12}$$

$$P_0\left(\left(\frac{C_T}{\sigma}\right)_{ref} = const., V_{tip} = const.\right) \propto \rho \tag{13}$$

$$P_p\left(\left(\frac{C_T}{\sigma}\right)_{ref} = const., V_{tip} = const.\right) \propto \rho \tag{14}$$

P_i being proportional to density by fulfilling the constraint of constant normalized blade loading, is one key aspect leading to the characteristics in figure 6 and figure 7. The dependence of P_i and ρ results in the same dependence concerning the main rotor power, the main-rotor torque and thus the tail-rotor thrust and total tail-rotor power. Summing up the power components for both main-rotor and tail-rotor results in P_{comp}, being a function of V_{tip} and with $P_{comp} \propto \rho$. Besides P_{comp} the required power contains the power components P_{acc} and P_{xmsn}. If P_{acc} and P_{xmsn} are assumed to be small regarding P_{req}, the ratio of P_i and P_0 is independent from ρ but it depends on rotor speed. Thus, the optimal rotor speed is approximately independent from ρ.

Within the NDARC UH-60A model, both the accessory losses and the transmission losses consist of constants and components scaled with density and rotor speed. Those components depending on rotor speed are proportional to density. This allows to rearrange all components equivalent to equation (15). P_1 consists of all components of P_{req} being proportional to density, whereas P_2 is its complement. Thus, P_2 is not proportional to ρ and P_2 is not a function of the main rotor speed. With these definitions the power savings ΔP_{req} and its derivative with respect to density in hover are:

(15) $$P_{req,ref/opt} = P_{1,ref/opt} + P_2$$

(16) $$\Delta P_{req} = \frac{P_{1,ref} - P_{1,opt}}{P_{1,ref} + P_2}$$

(17) $$\Rightarrow \frac{\partial\left(\Delta P_{req}\right)}{\partial\rho} = \frac{\Delta P_{req}}{P_{ref}}\left[\frac{P_2}{\rho} - \frac{\partial P_2}{\partial\rho}\right]$$

Despite P_2 is defined as not being proportional to ρ, $P_2 \propto \rho$ would result in $\partial\left(\Delta P_{req}\right)/\partial\rho = 0$. If $P_2 = 0$, it also follows $\partial\left(\Delta P_{req}\right)/\partial\rho = 0$. P_2 being independent from ρ would lead to the largest derivative, for example a constant power supply of accessory systems. In hover flight, within the engine limit it is: $\partial\left(\Delta P_{req}\right)/\partial\rho \approx 0..0.006$. At increased horizontal speed, $P_{comp} \propto \rho$ is no longer valid. This is due to a fundamental change of inflow principals and aerodynamic forces acting on non-rotating surfaces. Nevertheless, in the following examinations gross weight and altitude are substituted by $(C_T/\sigma)_{ref}$ as a good approximation at fast forward flight in accordance with figure 6. Power savings are namely increasing with density at a certain normalized blade loading at high cruise speed. That inhibits to conclude the altitude and gross weight from power savings at a certain normalized blade loading. By considering the full range of the normalized blade loading, it is guaranteed to cover the full potential of power savings.

Distinct phenomena of rotor aerodynamics are related to an increased flight speed. These typically include reverse flow, dynamic stall, compressibility, etc., which can be optimized by variable rotor speed in terms of efficiency. Thus, the horizontal flight speed and the normalized blade loading are the distinguished states, which reasonably represent the full flight envelope. In this sense, the power savings of the UH-60A are illustrated in figure 8. The horizontal flight speed is denoted as μ_{ref} instead of cruise speed, to be consistent with the dimensionless blade loading. The flight envelope is represented by the engine limit. Power savings up to 20% are possible within the flight envelope at low blade loading and the speed of maximal duration. As it was already discovered by [2] the maximal power savings can typically be gained at this speed, because the power P_0 is primarily reduced by optimal rotor speed and the ratio of P_0 towards P_{req} is at its maximum at the speed of best duration. As a result, the engine limit is mostly enlarged at this speed, too. The figure manifests a wide range where no power savings can be gained at approximately $(C_T/\sigma)_{ref} = 0.09..0.1$. This represents the design area of the UH-60A where the reference tip-speed of 725ft/sec is optimal. Obviously, the rotor speed optimum is adjusted towards forward flight conditions, rather than being designed towards hover efficiency. The design area is predominately aligned horizontally. Thus, power savings are essentially changing in blade loading direction and can be gained at high and low blade loading. The engine limit is extended in areas where power can be saved, especially at high normalized blade loading and high speed. The maximum flight speed increases by 3%. The normalized blade loading is approximately equal to maximum ceiling and gross weight improvements and increases by 6%. It should be noted that no envelope extensions are possible at the design area.

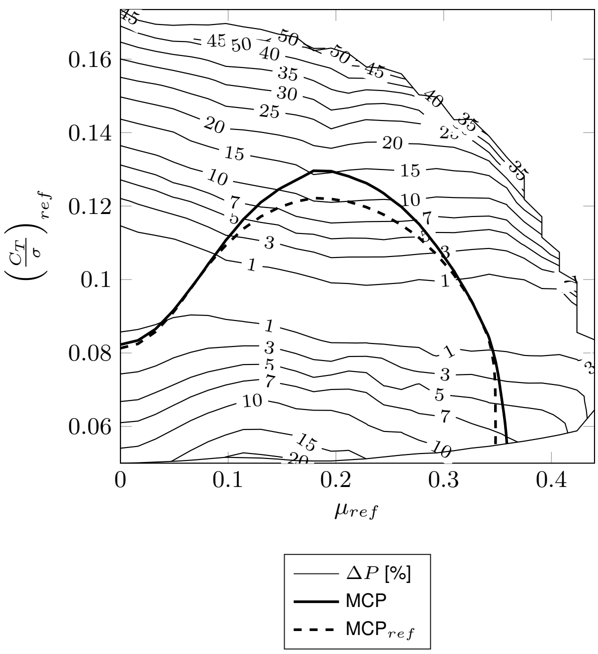

Figure 8: Power savings of the UH-60A helicopter over normalized blade loading and normalized advancing ratio. MCP is displayed for both optimal rotor speed and reference rotor speed.

The bandwidth of the optimal rotor speed ranges up from -30% to +10% within the engine limit, illustrated in figure 9. The change in rotor speed of 0% rep-

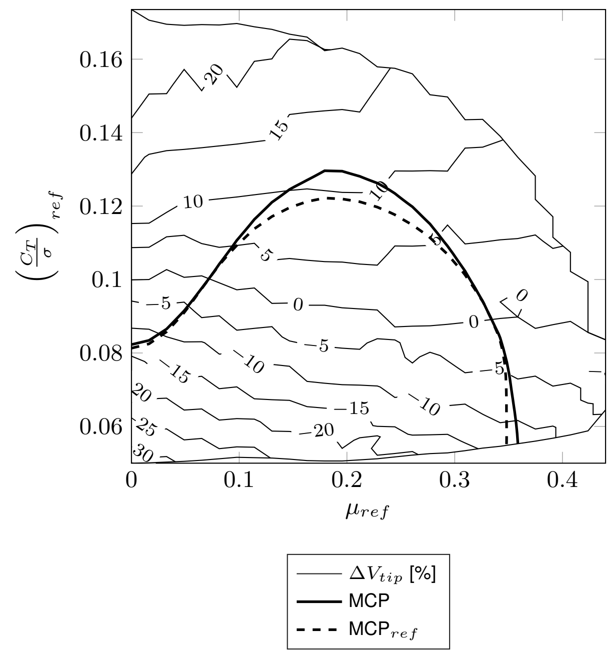

Figure 9: Optimal main-rotor tip-speed of the UH-60A helicopter compared to the reference main-rotor tip-speed.

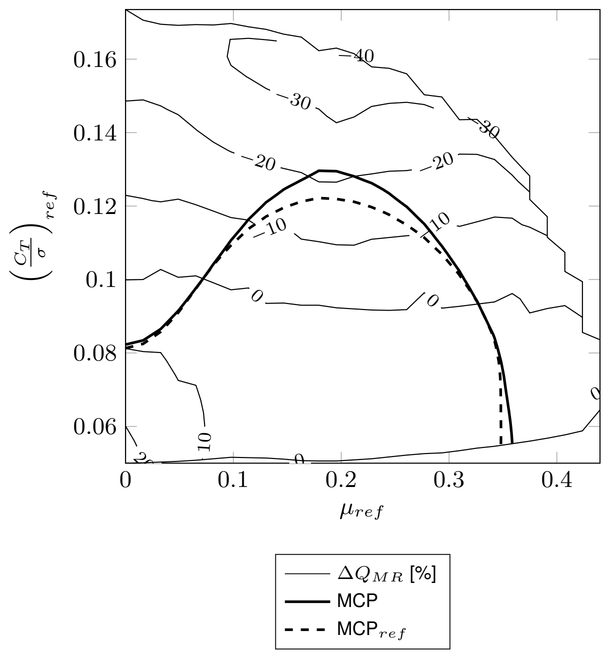

Figure 10: Change of mean main-rotor drive shaft torque of the UH-60A helicopter at optimal rotor speed compared to the reference rotor speed.

resents the already mentioned design area, where the reference rotor speed is optimal. Starting from low blade loading in hover, the optimal rotor speed increases with speed and blade loading. Obviously, it is more beneficial to address the flow conditions of the retreating blade, rather than of the advancing blade. This trend is inverted at $(C_T/\sigma)_{ref} \geq 0.11$. Thus, compressibility is no issue of the UH-60A that is needed to be addressed by variable rotor speed in terms of efficiency.

The main-rotor shaft torque is shown in figure 10. Again, the 0%-torque deviation represents the design area. Regarding this area, the torque decreases with respect to the torque of constant rotor speed at higher blade loading. At lower blade loading the main-rotor torque increases, especially at low flight speed. This trend is driven by the reduction of optimal rotor speed despite the reduction of power demand. Within the engine limit the maximum torque reduction is approximately -20% and the maximum torque increase is approximately +20%.

By using variable main-rotor speed the genuine blade loading spectrum can be reduced significantly to a range of approximate 0.08-0.12 from original 0.05-0.17 covering the same payload and altitude variations and the full speed range. The reduced C_T/σ-range does not approach the blade loading of minimal $c_{d,mean} \approx 0.05$. However, it approaches the optimal blade loading at reference tip-speed $(C_T/\sigma)_{opt} = 0.09..0.1$ of the overall helicopter. At optimal rotor speed the maximum advancing ratio occurring, increases from $\mu = 0.35$ to $\mu = 0.41$.

Optimal rotor speed characteristics of other configurations are illustrated in figure 12. As the results of the UH-60A are transferable to the other configurations in principal, particular differences with respect to the UH-60A are outlined in the following. The design rotor speed of the CH-47D, in contrast to the UH-60A, is located at a high blade loading with respect to the engine limit to enable the high payload capability. A reduction of the rotor speed by up to 15% would extend the flight speed by up to 20kts. However, the envelope can not be extended at high blade loading. The reference rotor speed of both the XH-59A helicopter and the XH-59A compound configuration is beyond the considered engine limit. As a result power savings are gained within the entire envelope. Furthermore, this leads to a speed limit extension of 10% without pusher propeller and 15% with pusher propeller, provided by a rotor speed reduction of 20%. This correlates with the implemented rotor speed reduction of the coaxial compound helicopter Sikorsky X2 [8]. Without pusher the minimum blade loading is increasing with flight speed. This is obtained to occur due to the stiff rotor system and the related pitch angle. This is resulting in an increase of normalized blade loading, to overcome fuselage drag. In helicopter mode the XV-15 shows an envelope extension in hover flight. In airplane mode the optimal rotor speed is reduced a lot. A rotor speed reduction of 50% is obtained with respect to the reference rotor speed in airplane mode of 600ft/sec (reference rotor speed in helicopter mode is 740ft/sec). The envelope is not covered completely by the calculation, but its extension at high speed can be obtained, rather than the extension of the maximum ceiling. The minimum speed limit results from the wings stall limit. The XV-15 requires the largest bandwidth of rotor speed. However, the variable rotor speed is useful to save power at corresponding flight states, rather than to extend the speed limit.

Except for the slender design area, where the reference rotor speed is optimal, power savings can be gained. However, the variable rotor speed technology is less beneficial by taking an additional transmission weight into account. The empty weight is increased to account for additional transmission weight as it is illustrated in figure 4. The transmission weight is assumed to increase by 10%. Furthermore, the increase of 30% is considered, to identify how additional weight impacts the beneficial regions within the envelope. The results are illustrated at 4 distinct altitudes in figure 13. The hatched areas illustrate the beneficial regions despite increased weight. Approximately, 65(45)% of the entire envelope are still beneficial, by taking 10(30)% additional transmission weight into account. The engine limit covers both regions of high and low blade loading, where power savings can be gained. The non-beneficial gross weight range is depending on altitude. This trend is driven by the optimal blade loading of the UH-60A. To achieve the optimal blade loading at low altitude the gross weight is higher than at high altitude. The non-beneficial region enlarged by increasing empty weight. As a result a certain rotor speed bandwidth is required at any flight speed in order to just be able to leave the non-beneficial region. If the variable rotor speed technology is still profitable, needs to be answered in the context of missions.

CONCLUSION AND OUTLOOK

The results are not indicating any inherent mistakes of the underlying models and the parameter settings. Nevertheless, the model should be considered to underestimate high μ phenomena, as the power savings at high speed are small against the expectations, especially regarding the lift-offset compound configuration. Furthermore, retreating blade phenomena should be considered as overestimated, as they provide unexpected, high improvements of efficiency by variable rotor speed. For that purpose high fidelity simulations should be conducted, but that would be far too extensive in order to cover the scope of this study.

Variable rotor speed is a promising technology to enhance efficiency and flight envelope. Up to 15% power reduction is possible within the engine limit. Operating at high altitude with high payload, at high speed or at the speed for maximal duration provides the most power savings, rather than the hover flight at high altitude or high gross weight. Depending on the configuration, a rotor speed bandwidth of $\pm$20% is required to achieve the power savings. A wide rotor speed range is especially required, by considering additional weight. Despite an increased empty weight to account for an additional variable transmission stage, power savings can still be gained.

The additional weight is difficult to forecast reliably. But certainly, this is important, as beneficial regions are sensitively depending on weight increase. Nevertheless, the increase of transmission weight should be ensured to stay below 30%. Apart from an additional transmission stage, the weight of the drive train is depending on the torque load. These loads change due to rotor speed variations. Thereby, a transmission weight reduction is not expected, because the flight envelope consists of both, regimes with increased and decreased torque. Torque is obtained to increases at low blade loading, vice versa and both conditions will be important for future helicopters.

The tilt rotor requires a widest range of rotor speed adjustment due to the change of flight mode. In contrast, no configuration sticks out regarding power savings. The most promising configuration for variable rotor speed purposes needs to be examined in a mission context. To use the full potential of the technology a new design should be conducted with respect to the design missions.

Apart from efficiency, the reduction of blade loading bandwidth, as it is obtained, is extending the thrust margin. Furthermore, rotor blade designs for variable rotor speed purposes are required to maintain a wide Mach-range rather than a wide angle of attack range. That is expected to result in vibrations, stability and controllability issues. Moreover, safety issues like a reduced autorotation-capability are needed to get addressed, as the optimal rotor speed is especially low in low altitude. It is pointed out that this has a positive effect on noise radiation.

In future, representative missions, derived from operators requirements, are considered to determine the related most beneficial configuration for further research on variable rotor speed. Subsequently, both a rotor system and a variable drive train will be designed and investigated towards the expected issues. The weight of the drive train is than resulting from design missions, time slices and related load spectra. Afterwards a proper blade concepts will be outlined.

ACKNOWLEDGMENT

Particular appreciations go to graduate student Daniel Eble and undergraduate student Emre Pancar contributing to this work during their theses. This work was supported by the German Federal Ministry for Economic Affairs and Energy through the German Aviation Research Program LuFo V-2 and the Austrian Research Promotion Agency through the Austrian Research Program TAKE OFF.

Supported by:

Federal Ministry for Economic Affairs and Energy

on the basis of a decision by the German Bundestag

FFG

Austrian Research Promotion Agency

References

[1] Misté, G. A., Benini, E., Garavello, A., and Gonzalez-Alcoy, M. "A Methodology for Determining the Optimal Rotational Speed of a Variable RPM Main Rotor/Turboshaft Engine System". In: *Journal of the American Helicopter Society* 60.3 (2015), pp. 1–11.

[2] Bowen-Davies, G. M. and Chopra, I. "Aeromechanics of a Variable-Speed Rotor". In: *American Helicopter Society 67th Annual Forum*. 2011.

[3] Khoshlahjeh, M and Gandhi, F. "Helicopter Rotor Performance Improvement with RPM Variation and Chord Extension Morphing". In: *American Helicopter Society 69th AHS Annual Forum*. 2013.

[4] Johnson, W., Yamauchi, G. K., and Watts, M. E. *NASA Heavy Lift Rotorcraft Systems Investigation*. NASA/TP-2005-213467 December. NASA Center for Aerospace Information, 2005, p. 106.

[5] Karem, A. E. *Optimum speed rotor*. Patent: US 6007298A. 1999.

[6] Amri, H., Feil, R., Hajek, M., and Weigand, M. "Possibilities and difficulties for rotorcraft using variable transmission drive trains". In: *CEAS Aeronautical Journal* 7.2 (2016), pp. 333–344.

[7] Ruddell, A. J. "Advancing Blade Concept (ABC^{TM}) Development". In: *Journal of the American Helicopter Society* 22.1 (1977), pp. 13–23.

[8] Blackwell, R and Millott, T. "Dynamics Design Characteristics of the Sikorsky X2 Technology^{TM} Demonstrator Aircraft". In: *64th Annual Forum Proceedings-American Helicopter Society* 64.1 (2008), p. 886.

[9] Johnson, W. "NDARC-NASA Design and Analysis of Rotorcraft Theoretical Basis and Architecture". In: *AHS Aeromechanics Specialists' Conference*. San Francisco, 2010.

[10] Johnson, W. "NDARC - NASA Design and Analysis of Rotorcraft Validation and Demonstration". In: *AHS Aeromechanics Specialists Conference 2010* February (2010), pp. 804–837.

[11] Bousman, W. G. and Kufeld, R. M. *UH-60A Airloads Catalog*. NASA/TM-2005-212827. Aeroflightdynamics Directorate (AMRDEC), 2005.

[12] Nagata, J. I., Piotrowski, J. L., Young, C., et al. *Baseline Performance Verification of the 12th Year Production UH-60A Black Hawk Helicopter*. Tech. Rp. AD-A208 671 85. Edwards Air Force Base, CA: Aviation Engineering Flight Activity, 1989, p. 75.

[13] Bender, G. L. *Airworthiness And Flight Characteristics Test (A&FC) of the CH-47D Helicopter*. Tech. Rep. AD-A151 380. Edwards Air Force Base, CA: USAAEFA, 1984, p. 244.

[14] Arents, D. *An Assessment of the Hover Performance of the XH-59A Advancing Blade Concept Demonstration Helicopter*. Tech. Rep. ASA042063. Fort Eustis, Va: U.S. Army Air Mobility Research and Development Laboratory, 1977.

[15] Ruddell, A. J. *Advancing Blade Concept (ABC) Technology Demonstrator*. Tech. Rep. ADA100181. Fort Eustis, Va: U.S. Army Research and Technology Laboratories, 1981.

[16] Ruddell, A. J. "Advancing Blade Concept (ABC) Development Test Program". In: *AIAA / SETP / SFTE / SAE / ITEA / IEEE 1st Flight Testing Conference*. Las Vegas, NV, 1981.

[17] Pleasants, W. A. *A Rotor Technology Assessment of the Advancing Blade Concept*. Tech. rep. 1983.

[18] Rand, O. and Khromov, V. “Compound Helicopter: Insight and Optimization”. In: *Journal of the American Helicopter Society* 60.1 (2015), pp. 1–12.

[19] Acree, C. W. and Tischler, M. B. *Determining XV-15 Aeroelastic Modes from Flight Data with Frequency-Domain Methods*. ATCOM Technical Report 93-A-004. 1993.

[20] Acree, C. W., Peyran, R. J., and Johnson, W. “Rotor Design Options for Improving Tiltrotor Whirl-Flutter Stability Margins”. In: *Journal of the American Helicopter Society* 46.2 (2001), pp. 87–95.

[21] Maisel, M. and Harris, D. “Hover Tests of the XV-15 Tilt Rotor Research Aircraft”. In: *AIAA / SETP / SFTE / SAE / ITEA / IEEE 1st Flight Testing Conference*. Las Vegas, NV, 1981, p. 15.

APPENDIX

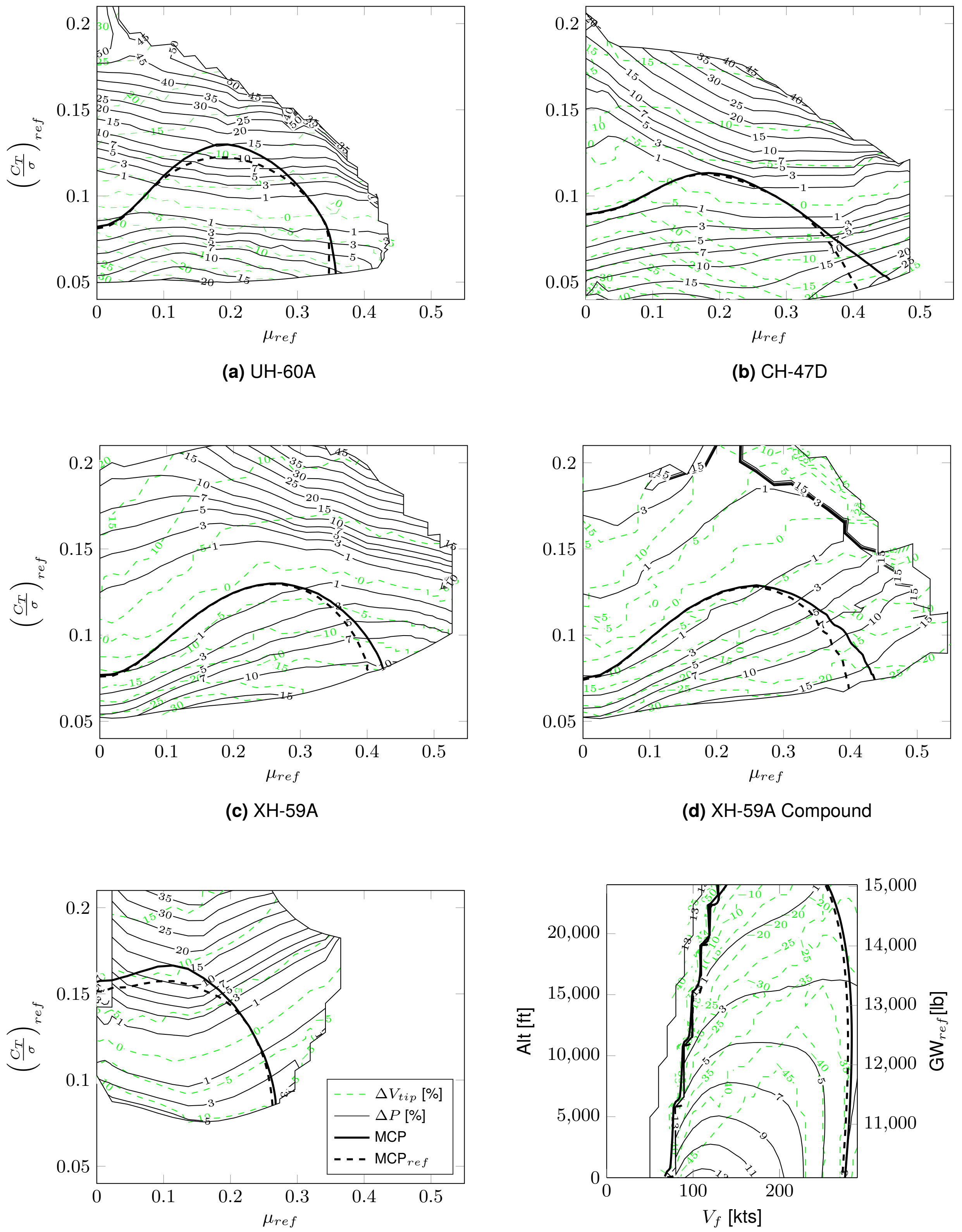

(a) UH-60A

(b) CH-47D

(c) XH-59A

(d) XH-59A Compound

(e) XV-15 helicopter mode

(f) XV-15 airplane mode

Figure 12: ΔP and ΔV_{tip} over blade loading $(C_T/\sigma)_{ref}$ and advancing ratio μ_{ref}. The maximum continuous power is shown for optimal rotor speed (MCP), as well as for reference rotor speed (MCP $_{ref}$).

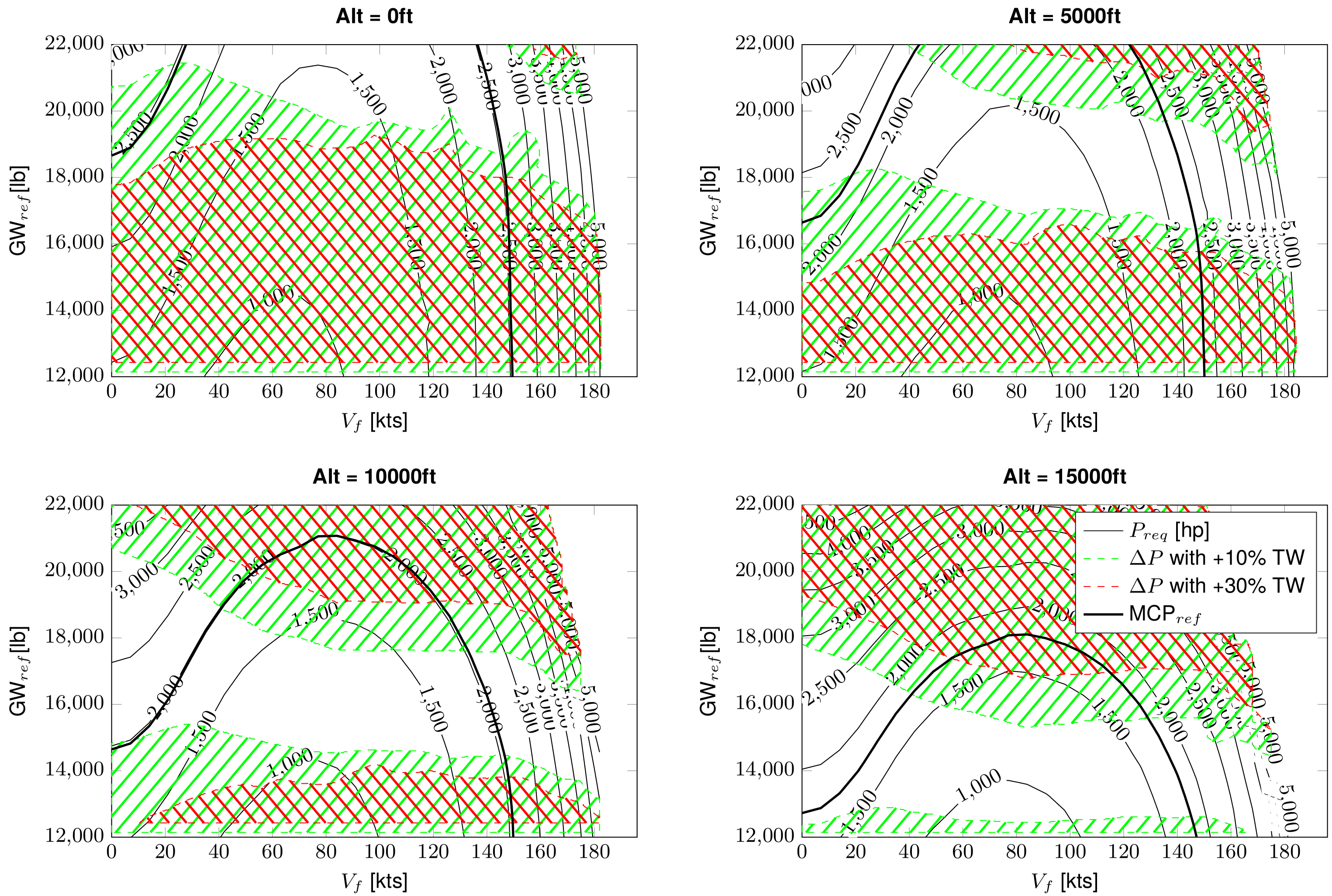

Figure 13: Required power of the UH-60A operating at design rotor speed.